Fulde-Ferrell Superfluids without Spin Imbalance in Driven Optical Lattices

Zhen Zheng, Chunlei Qu, Xubo Zou, and Chuanwei Zhang

Phys. Rev. Lett. **116**, 120403 — Published 24 March 2016

DOI: 10.1103/PhysRevLett.116.120403

Fulde-Ferrell superfluids without spin-imbalance in driven optical lattices

Zhen Zheng[1,2], Chunlei Qu[1], Xubo Zou[2], and Chuanwei Zhang[1]*
[1] *Department of Physics, The University of Texas at Dallas, Richardson, TX, 75080 USA*
[2] *Key Laboratory of Quantum Information, and Synergetic Innovation Center of Quantum Information & Quantum Physics, University of Science and Technology of China, Hefei, Anhui, 230026, People's Republic of China*

Spin-imbalanced ultra-cold Fermi gases have been widely studied recently as a platform for exploring the long-sought Fulde-Ferrell-Larkin-Ovchinnikov (FFLO) superfluid phases, but so far conclusive evidence has not been found. Here we propose to realize an FF superfluid without spin imbalance in a three-dimensional (3D) fermionic cold atom optical lattice, where s- and p-orbital bands of the lattice are coupled by another weak moving optical lattice. Such coupling leads to a spin-independent asymmetric Fermi surface, which, together with the s-wave scattering interaction between two spins, yields an FF type of superfluid pairing. Unlike traditional schemes, our proposal does not rely on the spin imbalance (or an equivalent Zeeman field) to induce the Fermi surface mismatch and provides a completely new route for realizing FF superfluids.

PACS numbers: 03.75.Ss, 67.85.-d, 74.20.Fg

The Fulde-Ferrell-Larkin-Ovchinnikov (FFLO) state, characterized by Cooper pairs with finite center-of-mass momenta [1, 2], is a central concept for understanding many exotic phenomena in different physics branches [3]. A crucial ingredient for realizing FFLO states is a large Zeeman field that induces Fermi surface mismatch of two paired spins [1, 2]. In recent years, FFLO states have been extensively studied in ultra-cold Fermi gases, where the population imbalance between two atomic internal states (pseudo-spins) serves as an effective Zeeman field [4–14]. Despite the intrinsic advantages of cold atoms compared to their solid state counterparts, conclusive evidence of FFLO states has not been found yet because of various obstacles. For instance, a large Zeeman field suppresses the superfluid order parameter, leading to a very narrow parameter region for FFLO states in 2D or 3D which can be easily destroyed by thermodynamic fluctuations [4–6]. In 1D, the parameter region for FFLO states could be large, but the quantum fluctuation is strong [7, 12, 14]. The recently proposed schemes using spin-orbit coupling and in-plane Zeeman field in a 3D Fermi gas may potentially overcome these obstacles [15–21] in principle, but they face practical experimental issues such as the large spontaneous photon emission from the near-resonant Raman lasers [22–31] and the strong three-body loss at Feshbach resonance in the presence of spin-orbit coupling [23–26].

In this Letter, we propose a new route for realizing FF superfluids in ultra-cold Fermi gases without involving population imbalance of two spin states that interact for generating Cooper pairing. Instead, we induce an asymmetric Fermi surface for the generation of FF states by other means and the populations of the two spins are fully equal. Our main results are the following:

1) We show that the s- and p_x-orbital bands of a 3D static optical lattice can be coupled using a weak 1D moving optical lattice along the x direction, which can be generated by two counter-propagating lasers with the frequency difference matching the s-p_x band gap. The s- and p_x-bands can be denoted as the band-pseudospin, and the moving lattice induces a band-pseudospin-momentum (i.e., spin-orbit) coupling and an in-plane Zeeman field, which yield an asymmetric Fermi surface along the x direction. The realization of such band-pseudospin-momentum coupling may provide a new platform for exploring exotic spin-orbit coupling physics.

2) We show that the asymmetric Fermi surface, together with the s-wave pairing interaction between two equally populated hyperfine spin states, can induce an FF type of Cooper pairing within a large parameter region in the 3D optical lattice, in sharp contrast to the narrow parameter region for the spin-imbalanced Fermi gas [6, 7]. Because of the 3D nature of the FF superfluids, the quantum fluctuations are also suppressed. The generated FF state is thermodynamically much more stable than the spin-imbalanced Fermi gas. Compared to the spin-orbit coupled schemes [15–21] that require near resonant Raman lasers [23–31], all lasers used here are far-detuned, therefore the proposed scheme should work for all types of fermionic atoms, including ^{6}Li [14]. Furthermore, because the hyperfine spins are not coupled with the momentum, the s-wave scattering interaction should be the same as regular Fermi gases without significant three-body loss at Feshbach resonance. These intrinsic advantages of our spin-balanced scheme make it experimentally more feasible than the spin-imbalanced schemes (with [4–14] or without spin-orbit coupling [15–21]), and thus may open a new route for observing FF superfluids.

Asymmetric Fermi surface in a driven optical lattice: Consider a degenerate spin-1/2 Fermi gas trapped in a static 3D optical lattice. Our proposed experimental setup is illustrated in Fig. 1(a). An additional 1D moving lattice along the x direction is applied to couple the s- and p_x-orbital bands of the static lattice. The moving lattice is generated by two counter-propagating lasers with a frequency difference of ω that matches the s-p_x band gap,

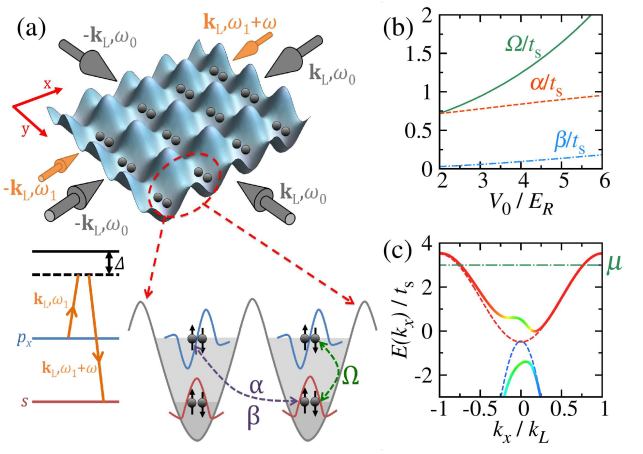

FIG. 1: (Color online) (a) An illustration of the experimental proposal: a moving lattice (orange arrows) induces effective two-photon Raman couplings between s- and p_x-bands of a 3D static optical lattice (only show 2D here, grey arrows). (b) Plot of different coupling strengths Ω, α and β as a function of the static lattice depth V_0. The moving lattice depth $V_x' = 0.8E_R$ with the recoil energy $E_R = h^2/2ma^2$. (c) The single-particle band structure for $V_0 = 3.0E_R$. $h = 5.5t_s$ and $\mu = 3t_s$ with $t_s = 0.111E_R$. The colors represent hybrid orbital compositions for each momentum state (red for s- and blue for p_x-orbital states). Dashed lines: bare s- and shifted p_x-orbital bands without coupling.

resulting in a two-photon Raman coupling between these two bands. All lasers are far-detuned to avoid heating from spontaneous emission. The overall time-dependent lattice potential can be written as

$$V(\boldsymbol{r},t) = \sum_{\eta=x,y,z} V_0\cos^2(k_L\eta) + V_x'\cos^2\left(k_Lx+\frac{\omega t}{2}\right), \quad (1)$$

where V_0 and V_x' are the static and moving lattice depths, $k_L = \pi/a$ with the lattice constant a.

We consider a large static lattice V_0, but a weak moving lattice V_x' (i.e., $V_x' \ll V_0$), therefore only on-site and nearest-neighbour tunnelings need be considered and the total wave function $|\Psi\rangle$ can be expanded in terms of the static lattice Wannier functions $|\Psi\rangle = \sum_j c_{sj}|s^j\rangle + c_{p_xj}|p_x^j\rangle$, where j is the site index in the x direction. $|s^j\rangle$ and $|p_x^j\rangle$ are the s-band and p_x-band Wannier functions at the j-th lattice site, c_{sj} and c_{p_xj} are their annihilation operators, respectively. Along the other two directions, p-band is not coupled and only s-band is considered and their related indices are neglected here for simplicity.

Under the Wannier basis, we can derive the single particle tight-binding Hamiltonian, where the time-dependence in the coupling between different orbits could be further eliminated using the rotating wave approximation [32], similar as the well-known two level Rabi oscillation. The difference from the Rabi oscillation is that the two levels here (s and p_x bands) have different band dispersions. Physically, there are three types of possible couplings between s and p_x bands, as illustrated in Fig. 1(a), with the coupling strengths given by $\Omega = \frac{V_x'}{4}\langle s^i|\sin(2k_Lx)|p_x^i\rangle$, $\alpha = \frac{V_x'}{2}\langle s^i|\cos(2k_Lx)|p_x^{i+1}\rangle$, and $\beta = \frac{V_x'}{2}\langle s^i|\sin(2k_Lx)|p_x^{i+1}\rangle$. The first term Ω denotes the coupling of two orbital states at the same site, while the last two terms α and β are the couplings between nearest neighbor sites [33]. The values of Ω, α, and β calculated from the Wannier functions are plotted in Fig. 1(b) (see also Fig. S1 [32]). β is usually small and not important for the physics discussed here.

The resulting time-independent single-particle Hamiltonian in the momentum space can be written as

$$H_0(\boldsymbol{k}) = \begin{pmatrix} \epsilon_s(\boldsymbol{k})+h & \Pi(k_x) \\ \Pi(k_x) & \epsilon_p(\boldsymbol{k})-h \end{pmatrix} \quad (2)$$

under the basis $(c_s(\boldsymbol{k}),\ c_{p_x}(\boldsymbol{k}))^T$, where $\Pi(k_x) = \Omega - \alpha\sin(k_xa) + \beta\cos(k_xa)$, $\epsilon_s(\boldsymbol{k}) = -2t_s[\cos(k_xa) + \cos(k_ya) + \cos(k_za)] - \mu$ and $\epsilon_p(\boldsymbol{k}) = 2t_p\cos(k_xa) - 2t_s[\cos(k_ya)+\cos(k_za)] - \mu$. t_s and t_p are the nearest neighbor tunneling amplitudes for atoms in the s- and p_x-orbital states, respectively. $2h$ is the energy difference between ω and the band gap Δ_g. μ is the chemical potential. Note that $\alpha\sin(k_xa)\sigma_x$ corresponds to the band-pseudospin-momentum coupling.

In the absence of α, $H_0(-\boldsymbol{k}) = H_0(\boldsymbol{k})$, revealing that the single-particle Hamiltonian is symmetric under inversion transformation. This inversion symmetry is broken when α and Ω coexist. A typical single-particle band structure, which is asymmetric along k_x-axis, is shown in Fig. 1(c). Here we just show the Fermi surface in the $k_{y,z} = 0$ plane. The Fermi surface is still symmetric along k_y and k_z directions. The orbital and hyperfine-spin degrees of freedom of the atoms are independent, therefore the coupling between different orbital states does not break the spin degeneracy and the hybrid bands are spin balanced at any $\boldsymbol{k}$ point.

Pairing Hamiltonian: Consider a spin-1/2 Fermi gas with equal spin populations loaded on such asymmetric orbital band. The dominant on-site atom-atom interaction between opposite spins can be made attractive via Feshbach resonance, similar as regular two component Fermi gases [34]. As a good approximation, the on-site atom-atom interaction can take the same form as the time-independent static system [32]. In the momentum space, the inter- and intra-band interaction term can be written as $H_{\rm int} = -\sum_{\mu\nu} g_{\mu\nu}c^\dagger_{\downarrow\mu}(\boldsymbol{k}_1)c^\dagger_{\uparrow\nu}(\boldsymbol{k}_2)c_{\uparrow\nu}(\boldsymbol{k}_3)c_{\downarrow\mu}(\boldsymbol{k}_4)$, where $\boldsymbol{k}_1+\boldsymbol{k}_2 = \boldsymbol{k}_3+\boldsymbol{k}_4$ due to the momentum conservation for the two-body scattering process. μ and ν denote the orbital states of two spins. $g_{\mu\nu} = g\int dx|w_\mu(x)|^2|w_\nu(x)|^2$ is the interaction coefficient for two atoms in two orbital states (labelled by μ and ν) and g is the two-body interaction strength in free space. To compare the strengths of the interactions between two orbital states, we approx-

imate the lattice potential at each site by a harmonic trap, which is a good approximation when the static lattice is not very weak. The relative ratio of the interaction strength is found to be $g_{ss} : g_{sp} : g_{ps} : g_{pp} = 1 : 0.5 : 0.5 : 0.75$ [32]. Hereafter we denote $g_{ss} = U$.

Under the mean-field approximation, we can rewrite the interaction term with the effective pairing between atoms. Because the inversion symmetry is broken for the single-particle Hamiltonian, the system may favor Cooper pairing with a finite center-of-mass momentum between two fermions of opposite spins. For simplicity, the chemical potential is chosen appropriately where there is only one simple Fermi surface (see Fig. 1(c)), therefore we could consider a plane-wave FF-type inter- and intra-band pairing $\Delta_{\mu\nu}(\mathbf{x}) = \Delta_{\mu\nu} e^{i\mathbf{Q}\cdot\mathbf{x}}$, similar as that in spin-orbit coupled system [15–21]. Here $\Delta_{\mu\nu} = g_{\mu\nu}\langle c_{\uparrow\mu}(\boldsymbol{Q}/2 + \boldsymbol{k}) c_{\downarrow\nu}(\boldsymbol{Q}/2 - \boldsymbol{k})\rangle$ denotes the amplitude of the s-wave order parameter between two orbital states μ and ν, and the FF vector $\boldsymbol{Q} = (Q, 0, 0)$ is the Cooper pairing momentum which is along the moving lattice direction. Note that the effective pairing on the asymmetric Fermi surface (Fig. 1c) could be $\boldsymbol{k}$-dependent (i.e., with non-s-wave components) due to the $\boldsymbol{k}$-dependent hybridization coefficients (determined by the eigenfunction of the Hamiltonian (2)) of two orbital bands for the asymmetric Fermi surface [35]. In the basis of spinor $(\Psi(\boldsymbol{Q}/2 + \boldsymbol{k}),\ \Psi^*(\boldsymbol{Q}/2 - \boldsymbol{k}))^T$ with $\Psi = (c_{\uparrow s}, c_{\downarrow s}, c_{\uparrow p_x}, c_{\downarrow p_x})^T$, the Bogliubov-de Gennes (BdG) Hamiltonian can be written as

$$H_{\mathrm{BdG}}(\boldsymbol{k}) = \begin{pmatrix} H_0(\frac{\boldsymbol{Q}}{2} + \boldsymbol{k}) \otimes \sigma_0 & \Delta_{4\times4} \\ \Delta^\dagger_{4\times4} & -H_0(\frac{\boldsymbol{Q}}{2} - \boldsymbol{k}) \otimes \sigma_0 \end{pmatrix}, \tag{3}$$

where σ_i $(i = x, y, z, 0)$ are the Pauli matrices,

$$\Delta_{4\times4} = \begin{pmatrix} \Delta_{ss} & -\Delta_{sp} \\ \Delta_{ps} & \Delta_{pp} \end{pmatrix} \otimes (-i\sigma_y)\ . \tag{4}$$

For each set of system parameters (V_0, V_x', U), the corresponding parameters Ω, α, β, t_s, t_p in the BdG Hamiltonian (3) are calculated from the Wannier functions, from which the order parameter amplitude $\Delta_{\mu\nu}$ and the FF vector $\mathbf{Q}$ are simultaneously obtained by minimizing the thermodynamic potential. When $\Delta_{\mu\nu} \neq 0$ and $Q \neq 0$, the system is in an FF phase. When $\Delta_{\mu\nu} \neq 0$, $Q = 0$, the system is in a BCS phase. Otherwise, the system is a normal gas.

Phase diagrams: In Fig. 2 we plot the intra-orbital order parameter Δ_{ss} and the Cooper pairing momentum Q with respect to the static and moving lattice depths V_0, V_x'. Δ_{sp} and Δ_{pp} are much smaller than Δ_{ss} [32], which is ascribed to the initial dominant populations of the s-orbital band at the position of the chemical potential. The s- and p_x-orbital band tunneling and coupling parameters (t_s, t_p, Ω, α) depend on the static lattice depth V_0 implicitly, therefore Δ_{ss} does not change monotonically. However, Ω and α depend on V_x' linearly,

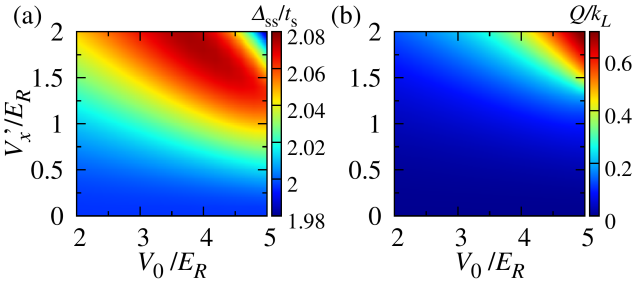

FIG. 2: (Color online) Phase diagrams of FF superfluids. The color describes the amplitude of (a) the order parameter Δ_{ss} and (b) the FF vector Q. Other parameters are $U = 6.0t_s$, $\mu = 10.0t_s$, $h = 8.0t_s$.

which directly determine the single particle band structure, therefore Q increases with increasing V_x'. Because the coupling between s- and p_x-orbital states does not depend on spins (the internal states) of atoms, Ω, α and β modify the energy dispersion in the same way for the two spins, leading to the spin degenerate asymmetric Fermi surface as shown in Fig. 1(c). Such spin-balanced asymmetric Fermi surface has little effect on suppressing the order parameter, in contrast to the strong suppression of the finite momentum pairing order induced by an external Zeeman field. Therefore Δ_{ss} is large and does not change much in the whole parameter region. Q is proportional to both Ω and α as shown in Fig. 2(b). When $V_x' = 0$, all the coupling coefficients vanish and the band inversion symmetry is preserved, thus the superfluid becomes a conventional BCS state.

When the on-site interaction U is tuned by changing the s-wave scattering length through Feshbach resonance, the system undergoes a BCS-BEC crossover. BCS-BEC crossover physics of Fermi gases has been widely studied in free space and in lattices [36, 37]. Here we present the phase diagram in the U-V_x' plane in Fig. 3. From Fig. 3(a), we see Δ_{ss} is mainly determined by the U and changes only slightly with the increase of moving lattice depth V_x'. FF states with large Q exist in a large param-

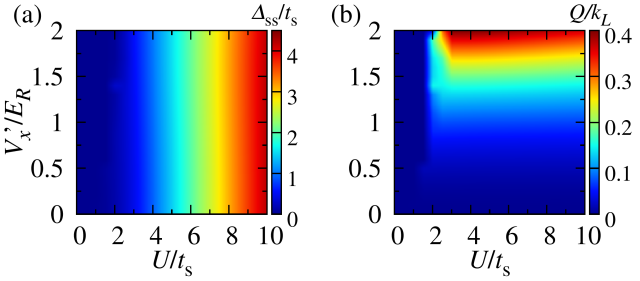

FIG. 3: (Color online) Phase diagrams in the BCS-BEC crossover. The color describes the amplitude of (a) the order parameter Δ_{ss} and (b) the FF vector Q. $V_0 = 4E_R$ with $t_s = 0.0855E_R$. Other parameters are $\mu = 10.0t_s$, $h = 8.0t_s$.

eter region which dominates when the moving depth is large. In the weak and medium interaction regimes, the order parameters are small and the ground state is mainly governed by the single-particle Hamiltonian. Therefore Q could be significant because of its sensitivity to the single particle dispersion. In the very strong interaction regime, the fermions form tightly bound molecules and the influence of the asymmetric energy dispersion on Cooper pairs is negligible. Therefore Q gradually decreases for a large U and the ground state eventually becomes a BCS state.

Stability of FF superfluids: The stability of the FF superfluid may be characterized by the thermodynamic potential difference $E_{\rm FF} - E_{\rm BCS}$ between the FF ground state and the possible BCS excited state (by enforcing $Q = 0$), which is shown in Fig. 4(a). The larger $|E_{\rm FF} - E_{\rm BCS}|$, the FF state is more stable. When $V_x' = 0$, the inversion symmetry is preserved and the FF superfluid becomes the BCS state, therefore $E_{\rm FF} = E_{\rm BCS}$. With the increasing V_x', $E_{\rm FF} - E_{\rm BCS}$ becomes negative, indicating that the asymmetric energy dispersion favors FF superfluids. In Fig. 4(b), we plot the thermodynamic potential E in the Δ_{ss}-Q plane for the premium values of Δ_{sp} and Δ_{pp} that minimize the total energy, which shows that the FF state is indeed the global minimum of the thermodynamic potential.

Compared with a Zeeman-field induced spin-imbalanced system, we find that the energy difference between the FF and BCS states in our system is one order of magnitude larger for the same interaction strength. Moreover, the FF states only exist in a very narrow Zeeman field parameter region ($\sim 10^{-2} t_s$) in the spin-imbalanced schemes and thus it is hard to find their signature experimentally. In contrast, the FF superfluids in our spin-balanced system exist in almost the whole parameter region.

Ω and α are proportional to the moving lattice depth V_x', and can be tuned in a wide parameter range to achieve an extremely asymmetric energy dispersion. In Fig. 4(a), we see $E_{\rm FF} - E_{\rm BCS}$ decreases sharply when V_x' is large. Therefore with a larger V_x', $|E_{\rm FF} - E_{\rm BCS}|$ may be much larger than that shown in Fig. 4(a), which is generally impossible in the spin-imbalanced Fermi gases. This advantage, together with the large parameter region for FF states, make our proposed spin-balanced Fermi gas experimentally more feasible for observing FF superfluids than the spin-imbalanced systems.

Experimental observation: The proposed FF superfluids can be realized with different types of fermionic atoms, such as ^{40}K and ^{6}Li. In the following, we illustrate the experimental setup and observation using ^{40}K. The ultra-cold ^{40}K gas with a spin-balanced mixture of internal states $|F, m_F\rangle = |9/2, -9/2\rangle$ and $|9/2, -7/2\rangle$ [52] is trapped in a 3D static optical lattice created by counter-propagating far-detuned lasers with wavelength $\lambda = 1064$ nm that defines the wavevector $k_L = 2\pi/\lambda$ and the recoil energy $E_R = \hbar^2 k_L^2/2m = 2\pi\hbar \times 4.5$ kHz.

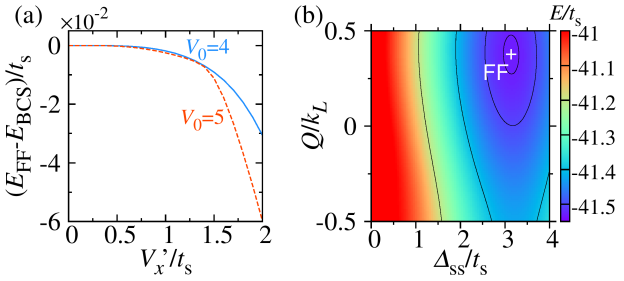

FIG. 4: (Color online) (a) The thermodynamic potential difference of the FF states and the possible BCS state as a function of V_x' for $V_0 = 4E_R$ (blue solid line, for which $t_s = 0.0855E_R$) and $V_0 = 5E_R$ (orange dashed line, for which $t_s = 0.0658E_R$). (b) The contour plot of the thermodynamic potential E in the Δ_{ss}-Q plane for $V_0 = 4.0E_R$, $V_x' = 2.0E_R$. The cross symbol corresponds to the self-consistent solution $\Delta_{ss} = 3.14t_s$, $Q = 0.377k_L$. Other parameters are $U = 8.0t_s$, $\mu = 10.0t_s$, $h = 8.0t_s$.

The lowest two orbital bands, s- and p_x-orbital, have a gap $\Delta_g \approx 2.6E_R$ when the static lattice depth is tuned as $V_0 = 3.0E_R$. The 1D moving lattice, created by another two counter-propagating lasers with a slight frequency difference of $\omega \sim \Delta_g/\hbar$, can be tuned to have a lattice depth of $V_x' = 0.1 \sim 0.8E_R$. With these parameters, the resulting coupling strengths have a range of $\Omega = 0.24 \sim 1.88t_s$ and $\alpha = 0.19 \sim 1.56t_s$ ($t_s = 0.111E_R$). The maximum value of FF momentum Q could be as large as $0.3k_L$ and the corresponding order parameter $\Delta \sim t_s$. Signatures of FF superfluids can be captured by the atom shot noise [38], or the sound speed measurement [39–41].

Discussion: In our spin-balanced system, only FF superfluids are possible because of the asymmetric s-p hybrid band structures. Even though the FF superfluid momentum $\mathbf{Q}$ could be gauged away from the order parameter's phase, $\mathbf{Q}$ is still revealed in the supercurrent of the system which is a gauge-invariant observable quantity [32]. The measurement of the supercurrent provides useful information of the system such as the s-p band coupling strength and the interaction strength.

Finally, we note that similar time periodic modulation of the lattices to generate exotic band structure, know as "Floquet engineering" [44–50], has been investigated extensively in experiments, leading to the observation of various important phenomena [42, 43, 51, 52], where the atomic spin states are irrelevant. However, the effects of s-wave interaction between two spins of the Fermi gas has not been well explored and our proposed FF superfluids showcase the rich quantum phases that may be generated by the s-wave two-body interactions in such Floquet systems. Our proposed band-pseudospin-momentum coupling in optical lattices may open a new avenue for exploring exotic spin-orbit coupling physics.

Acknowledgements: We thank Fan Zhang for help-

ful discussions. C. Qu and C. Zhang are supported by ARO (W911NF-12-1-0334), AFOSR (FA9550-13-1-0045), and NSF (PHY-1505496). Z. Zheng and X. Zou are supported by National Natural Science Foundation of China (Grants No. 11074244 and No. 11274295), and National 973 Fundamental Research Program (No. 2011cba00200).

Note added: After the submission of the manuscript, the modification of the band structure by the moving lattice has been observed experimentally with a BEC [53].

* chuanwei.zhang@utdallas.edu

[1] P. Fulde and R. A. Ferrell, Phys. Rev. **135**, A550 (1964).
[2] A. I. Larkin and Y. N. Ovchinnikov, Zh. Eksp. Teor. Fiz. **47**, 1136 (1964).
[3] R. Casalbuoni, and G. Narduli, Rev. Mod. Phys. **76**, 263 (2004).
[4] M.W. Zwierlein, A. Schirotzek, C.H. Schunck, and W. Ketterle, Science, **311**, 492 (2006).
[5] G. B. Partridge, W. Li, R. I. Kamar, Y. Liao, R. G. Hulet, Science, **311**, 503 (2006).
[6] H. Hu and X.-J. Liu, Phys. Rev. A **73**, 051603(R) (2006).
[7] X.-J. Liu, H. Hu, and P. D. Drummond, Phys. Rev. A **76**, 043605 (2007).
[8] M. M. Parish, S. K. Baur, E. J. Mueller, and D. A. Huse, Phys. Rev. Lett. **99**, 250403 (2007).
[9] J. Kinnunen, L. M. Jensen, and P. Törmä, Phys. Rev. Lett. **96**, 110403 (2006).
[10] K. Machida, T. Mizushima, and M. Ichioka, Phys. Rev. Lett. **97**, 120407 (2006).
[11] T. Koponen, J. Kinnunen, J.-P. Martikainen, L. M. Jensen, and P Törmä, New J. Phys. **8**, 179 (2006).
[12] H. Hu, X.-J. Liu, and P. D. Drummond, Phys. Rev. Lett. **98**, 070403 (2007).
[13] T. K. Koponen, T. Paananen, J.-P. Martikainen, and P. Törmä, Phys. Rev. Lett. **99**, 120403 (2007).
[14] Y.-A. Liao, A. S. C. Rittner, T. Paprotta, W. Li, G. B. Partridge, R. G. Hulet, S. K. Baur, and E. J. Mueller, Nature, **467**, 567 (2010).
[15] Z. Zheng, M. Gong, X. Zou, C. Zhang, and G. G. Guo, Phys. Rev. A **87**, 031602(R) (2013).
[16] F. Wu, G. Guo, W. Zhang, and W. Yi, Phys. Rev. Lett. **110**, 110401 (2013).
[17] C. Qu, Z. Zheng, M. Gong, Y. Xu, L. Mao, X. Zou, G. Guo, and C. Zhang, Nat. Commun. **4**, 2710 (2013).
[18] W. Zhang and W. Yi, Nat. Commun. **4**, 2711 (2013).
[19] X.-J. Liu and H. Hu, Phys. Rev. A **88**, 023622 (2013).
[20] C. Chen, Phys. Rev. Lett. **111**, 235302 (2013).
[21] L. Dong, L. Jiang, H. Hu, and H. Pu, Phys. Rev. A **87**, 043616 (2013).
[22] V. Galitski and I. B. Spielman, Nature **494**, 49 (2013).
[23] P. Wang, *et al.*, Phys. Rev. Lett. **109**, 095301 (2012).
[24] L. W. Cheuk, *et al.*, Phys. Rev. Lett. **109**, 095302 (2012).
[25] R. A. Williams, M. C. Beeler, L.J. LeBlanc, K. Jimenéz-García, and I. B. Spielman, Phys. Rev. Lett. **111**, 095301 (2013).
[26] Z. Fu, L. Huang, Z. Meng, P. Wang, L. Zhang, S. Zhang, H. Zhai, P. Zhang and J. Zhang, Nature Physics **10**, 110 (2014).
[27] Y.-J. Lin, K. Jimenéz-García, and I. B. Spielman, Nature **471**, 83-86 (2011).
[28] J.-Y. Zhang, *et al.*, Phys. Rev. Lett. **109**, 115301 (2012).
[29] C. Qu, C. Hamner, M. Gong, C. Zhang and P. Engels, Phys. Rev. A **88**, 021604(R) (2013).
[30] C. Hamner, C. Qu, Y. Zhang, J. Chang, M. Gong, C. Zhang and P. Engels, Nat. Commun. **5**, 4023 (2014).
[31] A. J. Olson, S.-J. Wang, R. J. Niffenegger, C.-H. Li, C. H. Greene, and Y. P. Chen, Phys. Rev. A **90**, 013616 (2014).
[32] See the Supplementary Materials.
[33] Because of different parities of the Wannier functions, the coupling between two orbital states at the same site mediated by $\cos(2k_L x)$ vanishes. The moving lattice also induces couplings between the same orbital states ($\mu = \nu$). These terms can also be eliminated by changing to the rotating frame coordinates after a unitary transformation [32].
[34] M. W. Zwierlein, C. A. Stan, C. H. Schunck, S. M. F. Raupach, A. J. Kerman, and W. Ketterle, Phys. Rev. Lett. **92**, 120403 (2004).
[35] C. Zhang, S. Tewari, R. Lutchyn, and S. Das Sarma, Phys. Rev. Lett. 101, 160401 (2008).
[36] Y. Ohashi and A. Griffin, Phys. Rev. Lett. **89**, 130402 (2002).
[37] E. Zhao and A. Paramekanti, Phys. Rev. Lett., **97**, 230404 (2006).
[38] M. Greiner, C. A. Regal, J. T. Stewart, and D. S. Jin, Phys. Rev. Lett. **94**, 110401 (2005)
[39] M. R. Andrews, D. M. Kurn, H.-J. Miesner, D. S. Durfee, C. G. Townsend, S. Inouye, and W. Ketterle, Phys. Rev. Lett. **79**, 553 (1997).
[40] J. Joseph, B. Clancy, L. Luo, J. Kinast, A. Turlapov, and J. E. Thomas, Phys. Rev. Lett. **98**, 170401 (2007).
[41] Y. Xu, R. Chu, and C. Zhang, Phys. Rev. Lett. **112**, 136402 (2014).
[42] M. Aidelsburger, M. Atala, M. Lohse, J. T. Barreiro, B. Paredes, and I. Bloch, Phys. Rev. Lett. **111**, 185301 (2013).
[43] H. Miyake, Georgios A. Siviloglou, Colin J. Kennedy, William Cody Burton, and Wolfgang Ketterle, Phys. Rev. Lett. **111**, 185302 (2013).
[44] N. Goldman and J. Dalibard, Phys. Rev. X **4**, 031027 (2014).
[45] N. Goldman, J. Dalibard, M. Aidelsburger, and N. R. Cooper, Phys. Rev. A **91**, 033632 (2015).
[46] L. D'Alessio and M. Rigol, Phys. Rev. X **4**, 041048 (2014).
[47] N. H. Lindner, G. Refael, and V. Galitski, Nat. Physics **7**, 490-495 (2011).
[48] Y. H. Wang, H. Steinberg, P. Jarillo-Herrero, and N. Gedik, Science **342**, 453-457 (2013).
[49] L. Jiang, *et. al.*, Phys. Rev. Lett. **106**, 220402 (2011).
[50] K. Jimenéz-García, L. J. LeBlanc, R. A. Williams, M. C. Beeler, C. Qu, M. Gong, C. Zhang, and I. B. Spielman, Phys. Rev. Lett. **114**, 125301 (2015).
[51] C. V. Parker, L.-C. Ha, and C. Chin, Nature physics **9**, 769 (2013).
[52] G. Jotzu, M. Messer, R. Desbuquois, M. Lebrat, T. Uehlinger, D. Greif, and T. Esslinger, Nature **515**, 237 (2014).
[53] M. A. Khamehchi, C. Qu, M. E. Mossman, C. Zhang, and P. Engels, arXiv:1506.03887